

# Challenges posed by statistical weights and data redundancies in iterative X-ray CT reconstruction

K. Schmitt, H. Schöndube, K. Stierstorfer, J. Hornegger, F. Noo

**Abstract**—Statistical iterative reconstruction methods are currently under extensive investigation for x-ray computed tomography. Among many options, the maximum likelihood solution is often preferred, particularly because it can be reduced to a weighted least-square problem. This solution may be sought using a moderate number of iterations of a specific algorithm such as Landweber’s method (or an ordered-subset variant of this algorithm), or may be sought with a penalty term and a number of iterations large enough to reach convergence. In the first case, the iteration number serves as a regularization means, whereas in the second case the penalty term defines the regularization procedure. It is well-known that the iteration number creates a (shift-variant) trade-off between resolution and noise, and that such a trade-off has been found useful in nuclear medicine. In this work, we show that the noise-resolution trade-off introduced by the iteration number is not always attractive for CT imaging, particularly when statistical weights and data redundancies are involved.

## I. INTRODUCTION

Statistical iterative reconstruction methods are currently under extensive investigation for x-ray computed tomography (CT), as they may offer significant gains in terms of image quality at equal dose, and thereby allow reduction in x-ray dose. There are many ways to formulate a statistical reconstruction method for x-ray CT. In particular, the maximum likelihood solution without and with constraints on the image appear both highly popular, particularly because finding this solution in CT can be reduced to a weighted least-square problem. In the first approach, the user formulates an iterative algorithm that converges towards the maximum likelihood solution and defines the reconstruction as the application of a finite number of iteration steps. Using this approach, the iteration number is essentially seen as a regularization means. Recall that the CT reconstruction problem is mildly ill-posed, so that regularization is essential to achieve satisfactory image quality. In the second approach, the regularization is not left to the iteration number; it is enforced directly by the constraint and the user iterates as long as needed to reach to minimum of the objective function. Popular constraints include the generalized Gaussian prior and the Huber penalty.

In this paper, we investigate the usefulness of the first approach for CT imaging, that is we study the effectiveness of regularization based on a finite number of iterations. Our study

K. Schmitt, H. Schöndube and K. Stierstorfer are with Siemens AG, Healthcare Sector. J. Hornegger is with the Pattern Recognition Lab, University of Erlangen-Nürnberg, Erlangen, Germany. F. Noo is with the Department of Radiology, University of Utah, Salt Lake City, Utah, USA.

The concepts presented in this paper are based on research and are not commercially available. This work was partially supported by NIH grant R01 EB007236; its content is solely the responsibility of the authors and do not necessarily represent the official views of the NIH.

includes essential aspects of CT imaging, namely non-uniform statistical weights and data redundancies.

## II. EXPERIMENTAL SETTING

### A. Data simulation

All simulations were performed in fan-beam geometry (3<sup>rd</sup> generation CT curved detector) using the FORBILD head phantom. Thus, each ray was parameterized by two angles,  $\lambda$  and  $\gamma$ , where  $\lambda$  is the polar angle specifying the source position and  $\gamma$  is the angle between the ray and the line that connects the source to the rotation center.

Full scans and short scans were both considered with parameters given in table 1. Also, note that a sub-sampling of each detector was employed to model the blurring that results from the finite size of the detector elements, and thereby mitigate high-frequency errors in the reconstruction. Specifically, each measurement was simulated as the average of five line integrals equally spaced over the detector width (non-linearities were neglected).

### B. Image representation and forward projection model

We decided to represent the attenuation function by its values on a Cartesian grid of points. The coordinates associated with this grid are called  $x$  and  $y$ . 350 by 350 locations were considered with a uniform sampling distance of 0.075 cm in both  $x$  and  $y$ .

The link between the attenuation function and the measurements was described using the principles of the distance-driven method [1]. That is, each line integral was evaluated as a simple sum in  $x$  or  $y$  together with a linear interpolation between grid points in  $y$  or  $x$ , respectively. As suggested by this method, note that the direction of summation was fixed for all lines within a fan-beam view, i.e., the position of the x-ray source defined the summation direction for all rays within the view. Also, the interpolation kernel accounted for both the sampling distance in  $\gamma$  and the sampling distance in  $x$  (or  $y$  depending on the interpolation direction).

### C. Reconstruction technique

Let  $c$  be the vector of unknown image coefficients, let  $g$  be the vector grouping the CT measurements, and let  $A$  be the matrix that links  $c$  to the CT measurements, as defined by the distance-driven method. Each reconstruction was performed using a moderate number,  $m$ , of iterations given by the following equation:

$$c^{(n+1)} = c^{(n)} + \eta \cdot A^T C^{-1} (g - A c^{(n)}) \quad (1)$$

where  $C$  is a constant diagonal matrix and  $\eta$  is a factor controlling convergence speed. The value for  $\eta$  was chosen as 0.90 times  $2/\sigma_{max}$  where  $\sigma_{max}$  is the maximum singular value of the matrix  $C^{-1/2}A$ , estimated using three iterations of the Power method [2]. The initial image vector,  $c^{(0)}$  was always chosen as the *zero* vector.

Conceptually, our iterative procedure can be interpreted as the application of Landweber's method to find the minimum-norm minimizer of

$$J(c) = \|C^{-1/2}(Ac - g)\|. \quad (2)$$

However, this minimizer was never reached since reconstruction was based on a moderate number of iterations. Recall that singular value decomposition analysis reveals that using a finite number of Landweber's iterations amounts to performing minimization with regularization. Given that the CT reconstruction problem is mildly ill-posed, regularization is actually essential. That is, the minimum-norm minimizer of  $J(c)$  is not attractive.

It is well-known that the iteration number generates a trade-off between resolution and noise. In PET imaging, this trade-off is often used to select the number of iterations. In this work, we will show that the resolution-noise trade-off induced by the number of iterations is unfortunately not often attractive for CT imaging, because it does not account for reconstruction errors other than resolution effects.

### III. RECONSTRUCTION WITH STATISTICAL WEIGHTS

In this section, matrix  $C$  is interpreted as the covariance matrix for the CT measurements. Because these measurements are assumed to be statistically independent,  $C$  is a diagonal matrix, with each element on the diagonal representing the variance of one measurement. This variance is equal to the inverse of the number of photons reaching the detector, which itself is influenced by the incoming number of photons, the shape of the bowtie filter and the attenuation property of the interrogated object.

#### A. Bowtie filter model

On x-ray CT scanners, the bowtie filter is a shaped piece of material (usually metal) which is placed between the x-ray source and the patient. It is designed to equalize the intensities of the rays hitting the detector for a given attenuating object. The primary purpose of the bowtie filter is to decrease the patient radiation dose near the edges of the scanning field-of-view (FOV) [3].

The effect of the bowtie filter is to make the number of photons going into the scanned object,  $N_{in}$ , vary with  $\gamma$ . In presence of a bowtie filter, we model the number of photons entering the interrogated object as

$$N_{in}(\gamma) = N_0 \cdot e^{-\eta(\gamma)}, \quad (3)$$

where  $N_0$  is the number of photons leaving the source and  $\eta(\gamma)$  is a function which models the effect of the bowtie filter.

Let  $\mu_{BF}$  be the linear attenuation coefficient for the bowtie filter and let  $d_{BF}$  be its thickness at  $\gamma = 0$ . Then  $\eta$  is defined as

$$\eta(\gamma) = g_{ob}(0) - g_{ob}(\gamma) + d_{BF} \cdot \mu_{BF}, \quad (4)$$

#### Fanbeam scanning parameters:

Source trajectory radius $R$	57 cm
Source to detector distance ( $D$ )	104 cm
Number of detector elements	340
Angular detector width ( $\Delta\gamma$ )	0.1368 radians

#### full scan:

Number of projections per turn	2320
--------------------------------	------

#### short scan:

Number of projections per turn	870
short-scan start angle $\lambda_s$	0 radians
short-scan stop angle $\lambda_e$	$3\pi/4$ radians
angular interval $d$	0, 5, 30

#### Bowtie filter:

Bowtie filter radius ( $r_{BF}$ )	8.0 cm
Bowtie filter attenuation ( $\mu_{BF}$ )	$0.54 \text{ cm}^{-1}$
Bowtie filter thickness parameter ( $d_{BF}$ )	0.50 cm

TABLE I

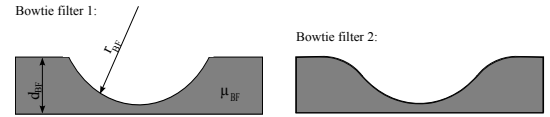


Fig. 1. Some examples for the shape of a bowtie filter.

where  $g_{ob}$  is the line integral through the object along the line  $L(\lambda, \gamma)$  for some fixed  $\lambda$ . Note that if the object is centered at the origin,  $\eta(\gamma)$  is circularly symmetric, and any fixed value of  $\lambda$  will suffice for the definition of  $g_{ob}$ .

#### B. Experiment details

A full scan acquisition with a bowtie filter is used. We consider two phantoms: the FORBILD head phantom and a simpler phantom that consists only of the outer two ellipses of the FORBILD head phantom. Figure 1 show two bowtie filters. Here, we used a bowtie filter shaped as bowtie filter 1 and 2, respectively. The value of each statistical matrix element is defined by  $C_{ij}^{-1} = N_{in} \cdot \exp(-\mu_W \cdot g_{m_{ij}})$ , where  $N_{in}$  are the remaining photons after the bowtie filter (Eqn. 3) to go through the phantom,  $\mu_W$  is the attenuation factor of water and  $g_{m_{ij}}$  is an element of the fan-beam data set. Bias was evaluated as the mean reconstruction error over pixels located within the dark ring in Fig. 5. The error for any given pixel was defined as the absolute difference between the reconstructed value and the true attenuation value of the hatched area, which is 50 HU.

#### C. Results

Figure 2 shows the reconstructed images for the two phantoms with bowtie filter 1 and bowtie filter 2, respectively. The number of the photons after bowtie filter 1 and bowtie filter 2 is shown in figure 3. Figure 4 shows the bias as a function of the iteration number for bowtie filter 1 and bowtie filter 2. Using bowtie filter 1 in our reconstruction algorithm (Eqn. 2) cause a ring artifact in the reconstructed images. This ring artifact can be traced back to the fact that the function  $N_{in}(\gamma)$  is not smooth since the radius of that ring has the same radius as the one of bowtie filter,  $r_{BF}$ . By iterating a very long time the thickness of the ring decrease. Finally, the ring disappears completely first after 1640 iterations. When we use a more complex phantom, we see similar artifacts

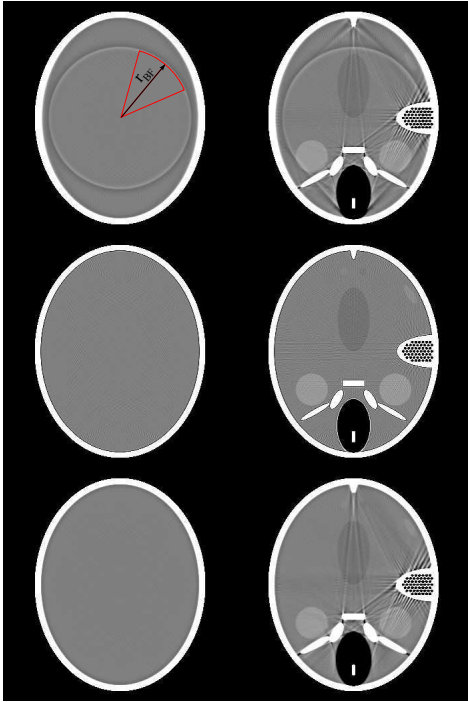


Fig. 2. Iterative reconstruction obtained from (first row) 250 iterations and (second row) 1640 iterations of the Landweber algorithm using bowtie filter 1, (third row) iterative reconstruction obtained from 250 iterations of the Landweber algorithm using bowtie filter 2. Grayscale: [1 1.1].

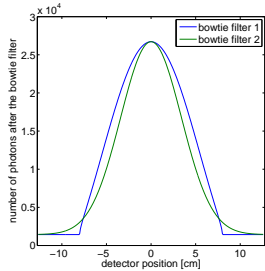


Fig. 3. Number of photons after the bowtie filter shown in Fig. 1 for different radius.

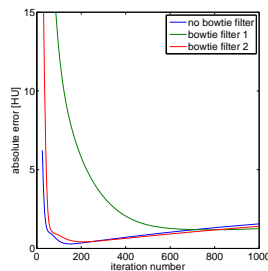


Fig. 4. Bias as a function of the iteration number by varying the number of iterations by steps of 5 beginning with 25 iterations.

appearing due to lack of smoothness in the statistical weights, but now replacement of the statistical weight with a smoother expression becomes a challenging question.

#### IV. DATA REDUNDANCIES

It is often the case that a CT scan involves redundant data. For example, each line integral is measured twice when a full scan is performed. However, not all line integrals are always measured the same number of times. In particular, when performing a short scan, some line integrals are measured twice whereas others are only measured once. In analytical reconstruction, non-uniform redundancies such as those encountered with the short scan need to be carefully addressed to avoid artifacts. A common approach is the utilization of a Parker-like weight. In iterative reconstruction, there is a priori no need to use such a weight, but, if desired this weight can be introduced as part of the definition of  $C$ . In this section, we assume that all measurements have the same variance, and

we study the impact of using a Parker-like weight for the definition of  $C$  versus using the identity matrix.

#### A. Data redundancy handling

To handle redundancies in the fan-beam data for the case of a short scan, we use a smooth weighting function

$$m(\lambda, \gamma) = \frac{c(\lambda)}{c(\lambda) + c(\lambda + \pi - 2\gamma)}, \quad (5)$$

where

$$c(\lambda) = \begin{cases} \cos^2\left(\frac{\pi(\lambda - \lambda_s - d)}{2d}\right) & \text{if } \lambda_s \leq \lambda < \lambda_s + d \\ 1 & \text{if } \lambda_s + d \leq \lambda < \lambda_e - d \\ \cos^2\left(\frac{\pi(\lambda - \lambda_e + d)}{2d}\right) & \text{if } \lambda_e - d \leq \lambda < \lambda_e \end{cases} \quad (6)$$

with  $d$  being the angular interval over which  $c(\lambda)$  smoothly drops from 1 to 0 [4]. If  $d$  is small, then the weighting function is similar to that of [5]. On the other hand, if  $d$  is large, then the weighting function is similar to Parker weighting [6].

#### B. Experiment details

In this second experiment, we investigate the influence of handling data redundancy in the Landweber algorithm. For this investigation, we created both full scan and short scan fan-beam data sets of the FORBILD head phantom. The data redundancy can be handled by setting the statistical matrix elements,  $C_{ij}^{-1}$ , equal to the result of Eqn. 5. We choose the angular interval  $d = 0, 5, 30$  in the function  $c(\lambda)$  in Eqn. 6, where  $d = 0$  means using no weights since  $m(\lambda, \gamma) = 1$ . For that experiment, we created additionally 10 noisy realizations of each fan-beam data set.

1) *Image quality*: Image quality was assessed in terms of resolution, bias and noise properties. Our noise measurements include the square root of the pixel variance,  $\bar{\sigma}$ . All bias and noise metrics were computed for the reconstructions obtained every fifth iteration.

2) *Resolution*: The modulation transfer function (MTF) was used to evaluate resolution. This function was obtained using a phantom that consists only of the central low contrast ellipse within the FORBILD head phantom (see Fig. 6, area 2). For any reconstruction of this phantom, an edge profile that gives the reconstructed value as a function of the distance from the ellipse is computed. Then, the MTF is obtained as the Fourier transform of the differentiated edge profile. Due to our linear reconstruction method, this approach is suitable to evaluate the resolution achieved within area 2 in Fig. 6.

Since the resolution varies from one image representation to the other and also changes at a different pace for each representation, we present all our figures of merit as a function of the mean MTF value. To obtain the mean MTF value, we computed the area under the MTF curve over the range defined by the Nyquist frequency for the data. This was done for every fifth iteration up to 1000 iterations.

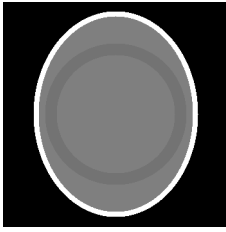


Fig. 5. The dark ring area was used for the calculation of the bias for the bowtie filter experiment.

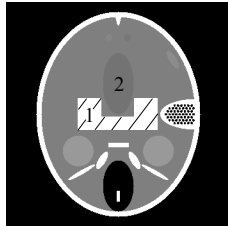


Fig. 6. The hatched area 1 was used for the calculation of the bias since this area is not affected by edge artifacts. Area 2 was used for the MTF calculation.

3) *Bias*: Bias was evaluated as the mean reconstruction error over pixels located within the hatched white area 1 in Fig. 6 since this area is not affected by edge artifacts. The error for any given pixel was defined as the absolute difference between the reconstructed value and the true attenuation value of the hatched area, which is 50 HU.

4) *Noise metrics*: The image noise was analyzed over a region of interest (ROI) that corresponds to the hatched area 1 in Fig. 6. The noise magnitude,  $\bar{\sigma}$ , was evaluated from pixel variance computations. Using our 10 noise realizations, we first subtract the bias image from the noisy image. Then, the pixel variance was estimated for each pixel location in the ROI. Afterwards, the results were averaged over all pixels in the ROI. The square root of this mean was defined as  $\bar{\sigma}$ .

### C. Results

Figure 7 shows the reconstructed images for the short scan case with an angular interval of  $d = 0, 5, 30$  and for the full scan case without and with noise. The bias metric and the mean standard deviation as a function of the mean MTF value is shown in Fig. 8 and in Fig. 9.

Taking data redundancy into account helps to reduce image artifacts in reconstructed short scan images. However, this has some strong side effects (Tab. II). On the one hand, the bias in the image can be reduced by some HU so that less iterations are required to obtain good looking images but on the other hand, the noise level is negatively influenced by that.

scan modus	iteration number to reach the mean MTF value 0.70	absolute error [HU]	mean std value $\bar{\sigma}$
full	240	1.07	50.63
short, $d = 0$	265	6.21	52.95
short, $d = 5$	385	3.37	61.18
short, $d = 30$	360	1.98	60.89

TABLE II

### V. CONCLUSIONS

We have shown in this work that utilizing the iteration number is rarely an effective means to regularize the reconstruction in x-ray CT imaging. As we have seen, both statistical weights and redundancies in the data set can easily introduce significant errors that differ from resolution errors and only disappear after a large number of iterations. Whereas the resolution reached after say 250 iterations may be deemed satisfactory, the user will generally observe that the image

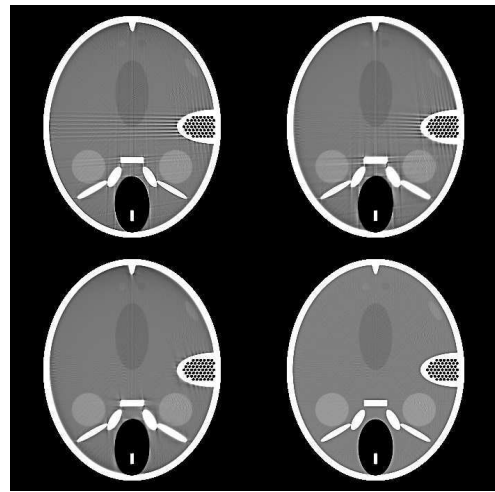


Fig. 7. Iterative reconstruction obtained from 250 iterations of the Landweber algorithm: (first row, left) in short scan geometry with  $d = 0$ , (first row, right) with  $d = 5$ , (second row, left) with  $d = 30$ , (second row, right) in full scan geometry. Grayscale: [1, 1.1].

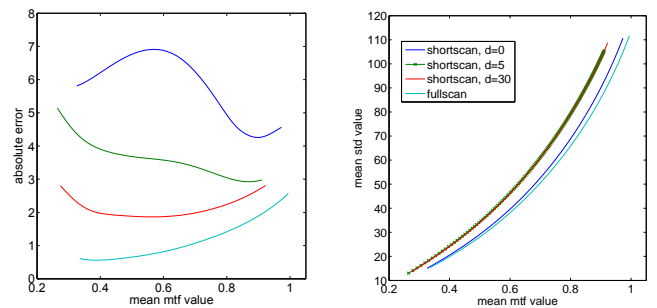


Fig. 8. Bias as a function of the mean MTF value obtained by varying the number of iterations by steps of 5 beginning with 50 iterations.

Fig. 9. Mean standard derivation as a function of the mean MTF value obtained by varying the number of iterations by steps of 5 beginning with 50 iterations.

quality is not. Hence, it is needed to iterate far beyond the desired resolution to first remove bias, and then post-smooth the result to attain the desired resolution. Under such circumstances, the penalized maximum-likelihood solution might be perceived as a more attractive reconstruction procedure. An alternative approach might be to initialize the reconstruction process with a filtered-backprojection procedure. However, in this case, it is important to understand what component of this first image remains when the reconstruction is completed.

### REFERENCES

- [1] B. De Man and S. Basu, "Distance-driven projection and backprojection in three dimensions," *Physics in Medicine and Biology* **49**, pp. 2463 – 2474, 2004.
- [2] G. H. Golub and C. F. van Loan, *Matrix Computations*, John Hopkins University Press, 1996.
- [3] J. Hsieh, *Computed Tomography Principles, Design, Artifacts, and Recent Advances*, SPIE Optical Engineering Press, 2003.
- [4] F. Noo, M. Defrise, R. Clackdoyle, and H. Kudo, "Image reconstruction from fan-beam projections on less than a short scan," *Phys. Med. Biol.* **47**, pp. 2525–46, 2002.
- [5] G.-H. Chen, R. Tokalkanahalli, T. Zhuang, B. E. Nett, and J. Hsieh, "Development and evaluation of an exact fan-beam reconstruction algorithm using an equal weighting scheme via locally compensated filtered backprojection," *Med. Phys.* **33**, pp. 475–81, 2006.
- [6] D. L. Parker, "Optimal short-scan convolution reconstruction for fan beam ct," *Med. Phys.* **9**, pp. 254–7, 1982.